

Article

Chromatography Denoising with Improved Wavelet Thresholding Based on Modified Genetic Particle Swarm Optimization

Jinhui Zhu , Zhongjun Fu , Keyang Li and Anjie Su

School of Computer Engineering, Jiangsu University of Technology, Changzhou 213001, China; dazaigugu@gmail.com (J.Z.); anque1932@gmail.com (K.L.); saj1996@126.com (A.S.)

* Correspondence: june@jsut.edu.cn

Abstract: The wavelet threshold functions are widely used in oil chromatography denoising because high-quality signals are the basis for Dissolved Gas Analysis (DGA), which determines the accuracy of transformer fault monitoring. However, there are certain limitations of the wavelet threshold functions, such as the Pseudo-Gibbs phenomenon and improper threshold selection. To this purpose, a modified genetic particle swarm optimization-based improved threshold function denoising method (MGPSO-ITF) is proposed. Specifically, the method constructs a new parametric threshold function that possesses high-order derivability and a small constant deviation. To obtain optimal values for the tunable parameters, MGPSO is employed, which outperforms other methods in identifying the optimum and achieving fast convergence. The simulation results demonstrate that the enhanced thresholding function yields a higher Signal-to-Noise Ratio (SNR), higher Noise Suppression Ratio (NSR), and smaller Root Mean Square Error (RMSE) compared to prior methods. Specifically, for the originally relatively smooth signal, MGPSO-ITF does not over-correct it to cause distortion. Furthermore, experiments on measured signals illustrate that the MGPSO-ITF is highly effective at denoising and preserving the original signal properties. Particularly in cases where peak deformation is prominent, the algorithm outperforms both hard and soft thresholding methods, achieving a reduction of 2.934% and 1.029% in peak area error, respectively.

Keywords: gas chromatography; genetic algorithms; particle swarm optimization; power transformers; signal denoising; wavelet transforms



Citation: Zhu, J.; Fu, Z.; Li, K.; Su, A. Chromatography Denoising with Improved Wavelet Thresholding Based on Modified Genetic Particle Swarm Optimization. *Electronics* **2023**, *12*, 4249. <https://doi.org/10.3390/electronics12204249>

Academic Editor: Cheng-Chi Lee

Received: 27 September 2023

Revised: 10 October 2023

Accepted: 11 October 2023

Published: 13 October 2023



Copyright: © 2023 by the authors. Licensee MDPI, Basel, Switzerland. This article is an open access article distributed under the terms and conditions of the Creative Commons Attribution (CC BY) license (<https://creativecommons.org/licenses/by/4.0/>).

1. Introduction

The transformer is one of the most important pieces of electrical equipment in the power system and the key to ensuring safe, efficient, and stable operation of the power system [1,2]. As a widely used insulating material, transformer oil is instrumental in insulation, heat conduction, and arc suppression [3]. By detecting the peak signals of various compounds through the chromatographic column, the type and content of different gases dissolved in the oil can be identified so as to determine the operating status and health condition of the transformer [4]. However, there tends to be significant noise and clutter interference in the chromatographic signal in actual engineering, which brings great difficulty to the chromatographic characterization and quantitative calculation. Consequently, potential faults in transformer operation may go undetected, posing safety risks [5–7].

There has been much research on effectively eliminating random noise in chromatographic signals, but most methods have inherent limitations. Median filtering and mean filtering techniques are inadequate for signals containing complex interference and uncertain factors [8,9]. Although Empirical Mode Decomposition (EMD) enables adaptive decomposition, it suffers from modal mixing [10]. Wavelet Transform (WT), by contrast, inherits and develops the idea of the localization of Short-time Fourier Transform (STFT) and has the characteristics of multi-scale analysis, low entropy, and de-correlation; so,

numerous filtering methods have been derived from WT [11]. Traditional filtering methods based on WT theory include wavelet modulus maxima, spatial correlation, and threshold function [12–14]. Additionally, Multistage Singular Spectrum Analysis (MSSA) is commonly employed [15,16]. Among the above methods, the hard thresholding denoising and the soft thresholding denoising proposed by Donoho are the most prevalent methods in actual engineering [17]. However, both threshold functions have certain defects, such as discontinuity of the hard threshold in the definition domain and constant deviation of the soft threshold. To solve these problems, scholars have proposed new threshold functions, which can be broadly categorized into non-parametric and parametric types. While non-parametric thresholding functions in Refs. [18,19] and exhibits improved denoising effects compared to traditional methods, they lack sufficient adaptive capabilities. Parametric thresholding functions, on the other hand, are proposed in Refs. [20–22], which can select parameters according to different situations to obtain better filtering effects. However, these selections still rely on empirical values.

In order to obtain the optimal parameters and increase interpretability, various optimization algorithms have been used, such as Genetic Algorithm (GA), Particle Swarm Optimization (PSO), and Artificial Bee Colony (ABC) [23–26]. Bhutada et al. [27] used PSO to minimize the Mean Square Error (MSE) between the expected and the output signals. While this approach yields a high Signal-to-Noise Ratio (SNR), its performance is limited by the lack of population diversity and its susceptibility to local optimum. Zhang [28] proposed a denoising method based on three dynamic strategies. This method improves the performance of PSO to a certain extent and is verified in the test signal. Yang et al. [29] proposed a new threshold function denoising method using relative wavelet entropy as the fitness function. Although the resulting denoised simulation signal exhibits improved smoothness, the effectiveness is not significant in actual signal verification. Wang et al. [30] proposed an ABC algorithm based on a good point set and dynamic elite group guidance combined with simulated annealing selection. This method demonstrates superior performance in achieving optimal threshold values, albeit with increased computational complexity.

To summarize, the primary challenges that must be addressed pertain to the construction and determination of threshold functions in denoising applications. First, the lack of established guidelines for threshold function construction poses a significant obstacle. Secondly, the iterative process of determining threshold function parameters can lead to decreased population diversity, resulting in suboptimum and less effective denoising outcomes. Therefore, an improved threshold function denoising algorithm based on modified genetic particle swarm optimization (MGPSO-ITF) is proposed in this paper. The contributions of this paper are as follows:

- To address the limitations of traditional threshold functions, we propose the ITF with high-order derivability, negligible constant deviation, and continuous definition domain. These strengths make it an attractive choice for signal-processing applications. Meanwhile, MGPSO is utilized to obtain the optimal threshold parameters, which improves the estimation precision of the threshold parameters.
- The three improvements of the MGPSO algorithm are as follows: (1) MGPSO takes PSO as the main body and GA as the auxiliary. In the early stage, the particles are updated separately through PSO. Once the algorithm reaches a local optimum, the GA selection, crossover, and mutation are utilized to update particles and escape the local optimum. (2) The algorithm modifies the PSO strategy with nonlinear inertia weights and learning factors, thereby accelerating the convergence speed of PSO. (3) Adaptive mutation probability and multi-point crossover operations between particles and personal best value (pbest) are employed to enhance the global optimization efficiency of GA.
- The experimental results demonstrate that the MGPSO-ITF offers the following advantages: In simulation experiments, the algorithm outperforms other methods by achieving a smaller Root Mean Square Error (RMSE), higher SNR, and higher Noise Suppression Ratio (NSR) across various levels of Gaussian white noise interference. In the measured signal experiment, the proposed algorithm is significantly improved

compared with the traditional chromatographic denoising method. The algorithm not only effectively reduces noise but also minimizes errors in the chromatographic peak area, while preserving the original signal characteristics to their maximum.

The rest of the paper is organized as follows: Section 2 presents the theory background. Section 3 presents the proposed MGPSO-ITF algorithm. Sections 4 and 5 verify the effectiveness of the MGPSO-ITF using the simulated and measured signals, respectively. Section 6 concludes the paper.

2. Wavelet Threshold Denoising Theory Background

Discrete wavelet transform (DWT) is an effective multi-scale analysis algorithm that achieves signal analysis by decomposing the signal into approximate coefficients and detail coefficients at different scales. In the DWT algorithm, we can obtain the wavelet function by scaling and translating the mother wavelet, such as Equation (1), where a and b represents the scaling factor and translation factor, respectively, and $j, k \in Z$.

$$\varphi_{j,k}(t) = |a|^{-\frac{j}{2}} \varphi\left(a_0^j t - kb_0\right). \quad (1)$$

According to Equation (1), we can obtain the high-frequency coefficients and low-frequency coefficients of discrete wavelet decomposition, as shown in Equations (2) and (3), respectively, where $*$ stands for the conjugate operation.

$$d_{j,k} = \langle f(t), \varphi_{j,k} \rangle = |a_0|^{-\frac{j}{2}} \int_{-\infty}^{+\infty} f(t) \varphi^*\left(a_0^{-j} t - kb_0\right) dt \quad (2)$$

$$a_{j,k} = \langle f(t), \phi_{j,k} \rangle = |a_0|^{-\frac{j}{2}} \int_{-\infty}^{+\infty} f(t) \phi^*\left(a_0^{-j} t - kb_0\right) dt \quad (3)$$

Inherent to the noise, it exhibits a prominent concentration in the high-frequency wavelet coefficients. Conversely, the energy of the signal primarily resides in the low-frequency wavelet coefficients. In the domain of chromatographic signals, they can be conceptualized as a composite of a low-frequency pure signal and high-frequency noise.

$$f_i = x_i + s_i \quad i = 1, 2, \dots, N, \quad (4)$$

where f_i is the chromatographic signal, x_i is the pure signal, s_i is the background noise, and N is the total number of samples. The method of wavelet threshold denoising includes the following three steps:

- Choose the appropriate wavelet basis function and the number of decomposition layers for multi-scale decomposition of f_i to obtain its high-frequency coefficients and low-frequency coefficients;
- Process the wavelet coefficients using the threshold function;
- Reconstruct the signal using the Inverse Discrete Wavelet Transform (IDWT) algorithm.

Figure 1 clearly shows the process of decomposing, thresholding, and reconstructing a signal using DWT, where j is the number of decomposition layers, cA is the low-frequency coefficient, and cD is the high-frequency coefficient. Among the thresholding phases depicted in the figure, the widely employed methods include hard thresholding and soft thresholding. Nevertheless, both traditional thresholding methods are not without inherent drawbacks.

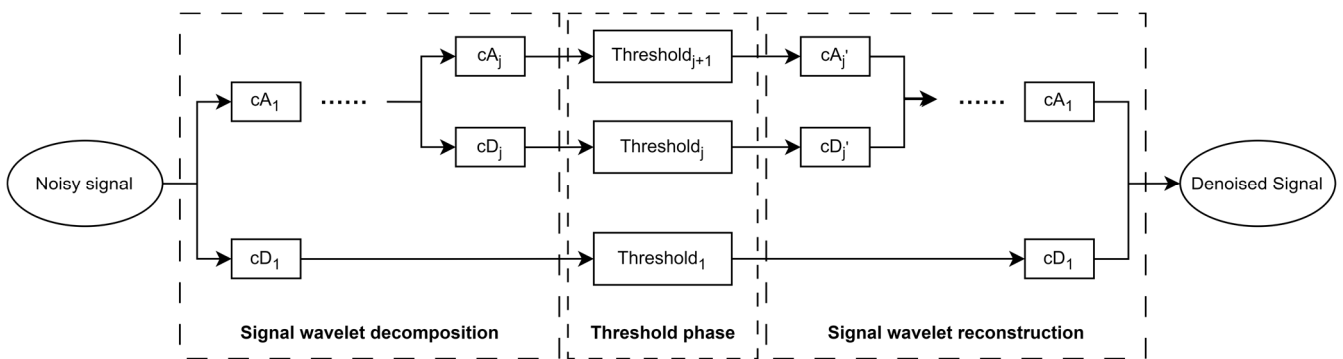


Figure 1. Wavelet decomposition and reconstruction of the signal.

In hard thresholding, the deviation between the reconstructed signal and the original signal equals zero, but the function is discontinuous at the threshold point. This situation will lead to severe oscillations; so, the application of such thresholding is limited. The expression of the hard thresholding function is

$$\hat{w}_{j,k} = \begin{cases} w_{j,k}, & |w_{j,k}| \geq \lambda \\ 0, & |w_{j,k}| < \lambda \end{cases} \quad (5)$$

where $w_{j,k}$ is the original wavelet coefficient, $\hat{w}_{j,k}$ is the processed wavelet coefficient, and λ is the threshold.

In soft thresholding, continuity is improved. The wavelet coefficients are reduced using a fixed threshold, and this constant deviation phenomenon leads to the loss of some useful high-frequency information. The expression of the soft thresholding function is

$$\hat{w}_{j,k} = \begin{cases} \text{sgn}(w_{j,k}) (|w_{j,k}| - \lambda), & |w_{j,k}| \geq \lambda \\ 0, & |w_{j,k}| < \lambda \end{cases} \quad (6)$$

Therefore, it is evident that a superior threshold function must both possess high-order differentiability in the wavelet domain and minimize the discrepancy between the estimated coefficients and their original counterparts. Diverse processing strategies and estimation methods for wavelet coefficients have a direct impact on the final denoising outcome. These techniques significantly influence the effectiveness of noise reduction and play a pivotal role in achieving superior denoising results.

3. The Chromatography Signal Denoising Algorithm MGPSO-ITF

In order to effectively reduce the influence of Gaussian noise on the chromatographic signal, a new signal-denoising algorithm is proposed by combining the ITF and the optimization method of MGPSO. The algorithm is described in detail below.

3.1. Construction of a New Threshold Function

Aimed at remedying the shortcomings of traditional thresholding, an improved threshold function is proposed to process the oil chromatography monitoring signal. The expression of the improved threshold function is

$$\hat{w}_{j,k} = \begin{cases} \text{sgn}(w_{j,k}) \left(|w_{j,k}| - \frac{\lambda}{\alpha^{\beta(\sqrt{|w_{j,k}|/\lambda}-1)}} \right), & |w_{j,k}| \geq \lambda \\ 0, & |w_{j,k}| < \lambda \end{cases} \quad (7)$$

where α and β are custom tuning parameters in the range of $[1, +\infty]$. α controls the shape of the threshold function, which becomes the soft threshold function when $\alpha = 1$ and becomes the hard threshold function when $\alpha \rightarrow +\infty$. β is an exponential factor that controls how quickly the threshold function changes from soft thresholding to hard thresholding.

The improved function is a transitional function constructed based on a power function with an independent variable of α . It has high-order derivability that eliminates oscillations and smooths the reconstructed signal. The continuity, deviation, and asymptote of this function are demonstrated in detail below.

3.1.1. Continuity

The function is a piecewise function and its definition domain is divided into three parts: $(-\infty, -\lambda)$, $(-\lambda, +\lambda)$, $(+\lambda, +\infty)$. Since the function is continuous within all three parts, to prove that the function is continuous, it is only necessary to prove that the left and right limits of the segmented points are equal and are equal to the function value.

$$\lim_{w_{j,k} \rightarrow (-\lambda)^-} \hat{w}_{j,k} = \lim_{w_{j,k} \rightarrow (-\lambda)^+} \hat{w}_{j,k} = 0, \tag{8}$$

$$\lim_{w_{j,k} \rightarrow \lambda^-} \hat{w}_{j,k} = \lim_{w_{j,k} \rightarrow \lambda^+} \hat{w}_{j,k} = 0. \tag{9}$$

Evidently, when $w_{j,k} = \pm\lambda$, $\hat{w}_{j,k} = 0$. Combining Equations (8) and (9), it can be seen that the left and right limits of the segmented points are equal and are equal to the function value; so, the threshold function is continuous in the definition domain, which theoretically overcomes the defects of hard thresholding.

3.1.2. Deviation

The deviation of this threshold function is calculated as

$$\lim_{w_{j,k} \rightarrow +\infty} (\hat{w}_{j,k} - w_{j,k}) = 0, \tag{10}$$

$$\lim_{w_{j,k} \rightarrow -\infty} (\hat{w}_{j,k} - w_{j,k}) = 0, \tag{11}$$

it follows when $x \rightarrow \infty$, $\hat{w}_{j,k} \rightarrow 0$. This means the bias is reduced as much as possible.

3.1.3. Asymptote

Expression Equation (12) implies that $\hat{w}_{j,k} = w_{j,k}$ is the asymptote of the threshold function. This conclusion also corroborates with the above deviation proof, which theoretically succeeds in overcoming the defects of soft thresholding.

$$\lim_{w_{j,k} \rightarrow -\infty} \left(\frac{\hat{w}_{j,k}}{w_{j,k}} \right) = \lim_{w_{j,k} \rightarrow +\infty} \left(\frac{\hat{w}_{j,k}}{w_{j,k}} \right) = 1. \tag{12}$$

Figure 2 compares the images of the thresholding function with different parameters when $\lambda = 1$. It is clear that the improved threshold function is a compromise strategy between soft thresholding and hard thresholding, which is adjusted according to α, β , and makes use of the function more flexibly. It is continuous and smooth while preserving larger wavelet coefficients, which means the threshold function in Equation (7) is more faithful to the original signal.

3.2. Parameter Optimization Based on MGPSO

Traditional threshold estimation methods that rely on a unified threshold are limited by the accuracy of noise-variance estimation. If the threshold is set too small, the resulting denoised signal will still contain noise, while if it is set too large, the reconstructed signal will be distorted. In order to improve the estimation accuracy of the threshold, α, β and λ in Equation (7) are considered as unknown threshold parameters and optimized using the MGPSO method. This approach offers a more effective way to estimate the threshold, as it reduces the reliance on accurate noise-variance estimation. MGPSO takes PSO as the main body and GA as the auxiliary. The operation of the algorithm can be divided into the following three stages.

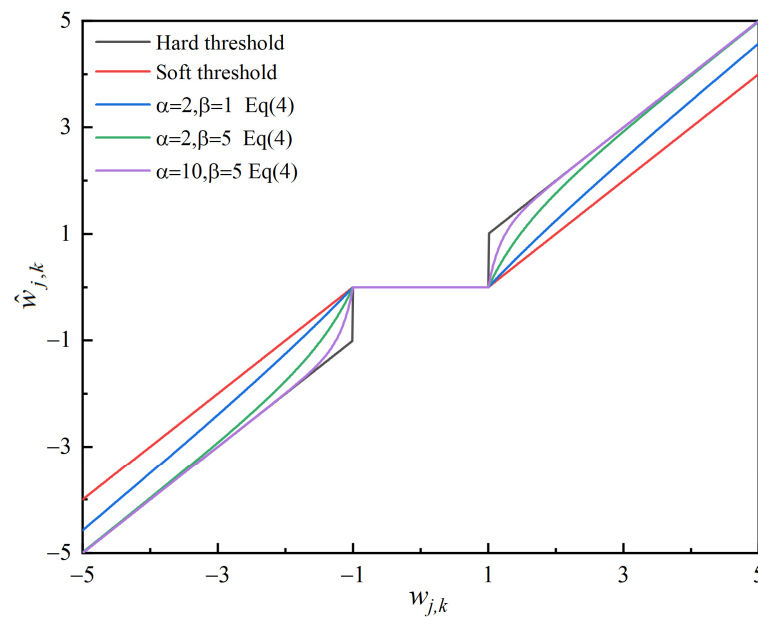


Figure 2. Images of different threshold functions when $\lambda = 1$.

3.2.1. Rapid Iteration through PSO

PSO is a swarm intelligence computing technology inspired by the group behavior of birds. Compared with other evolutionary algorithms, the principle of particle swarm optimization is simple. It has a memory function and requires adjusting fewer parameters, making it suitable for the early stage [31]. The mathematical model is as follows:

$$v_{ij}^{t+1} = w_t \times v_{ij}^t + c_1 r_{1ij} (pb_{ij}^t - x_{ij}^t) + c_2 r_{2ij} (gb_{ij}^t - x_{ij}^t), \tag{13}$$

$$x_{ij}^{t+1} = x_{ij}^t + v_{ij}^{t+1}, \tag{14}$$

where t is the current number of iterations, j is the current solution space, r_1, r_2 are two random numbers in the range of $[0, 1]$, w is the inertia weight coefficient, and c_1, c_2 are the learning factors. In order to improve the convergence speed and accuracy of PSO, we follow two particular strategies.

For the inertia weight, the larger its value, the stronger the global search ability; the smaller its value, the stronger the local search ability. A nonlinear decreasing strategy is adopted in this stage, which has a search characteristic in the form of a parabolic. This strategy is beneficial to improve the convergence speed and accuracy of the algorithm, which can be expressed as

$$w_t = w_{\max} - (w_{\max} - w_{\min}) \left(\frac{2t}{t_{\max}} - \left(\frac{t}{t_{\max}} \right)^2 \right). \tag{15}$$

The learning factor controls the direction and step size of the particles moving to the pbest and the global best value (gbest). This modified strategy, inspired by Ref. [32], replaces the learning factors in PSO with sine and cosine terms. With this method, the global exploration and local exploitation of the algorithm can be better balanced, thus improving the search accuracy. The expression for this modified strategy is as follows:

$$r_3 = 2 - \frac{2t}{t_{\max}}, \tag{16}$$

$$c_1 = c_2 = \begin{cases} r_3 \sin(r_4), & r_5 < 0.5 \\ r_3 \cos(r_4), & r_5 \geq 0.5 \end{cases}, \tag{17}$$

where r_4 is a random number in the range of $[0, \pi/2]$ and r_5 is a random number in the range of $[0, 1]$.

3.2.2. Mitigating the Local Optimum through the Crossover

Due to the poor diversity of PSO populations, it is easy to fall into a local optimum, which occurs more frequently when dealing with high-dimensional complex problems. When the gbest does not change for many consecutive times, it is considered that PSO iterates to a suboptimal solution, at which point it enters the second stage. The modified algorithm sorts the fitness values of the particles and selects the particles with better fitness to crossover with the pbest. The principle is simple and easy to understand, and the position of new particles is updated by Equation (18) as follows:

$$x_{ij}^{t'} = r_6 x_{ij}^t + (1 - r_6) p b_{ij}^t \quad (18)$$

where $x_{ij}^{t'}$ is the particle position after the crossover operation, x_{ij}^t and $p b_{ij}^t$ are the parents selected based on fitness values and the pbest, and r_6 is a random number in the range of $[0, 1]$.

3.2.3. Further Population Expansion through the Mutation

If successive crossover operations do not result in gbest changes, the algorithm requires a more significant population change, at which point it enters the third stage. It updates particles using uniform mutation based on the adaptive mutation probability, which allows the search points to move freely throughout space, thus increasing the diversity of the population dramatically. Once the gbest changes, it indicates that the operation helps the algorithm jump out of the local optimum solution, as suggested, and the relevant equation is as follows:

$$x_{ij}^{t'} = x_{ij\min}^t + r_7 (x_{ij\max}^t - x_{ij\min}^t) \quad (19)$$

$$p_m = \eta \cdot p_{m\max} \quad (20)$$

$$\eta = \frac{t}{t_{\max}} \quad (21)$$

where x_{ij}^t is the mutation point, r_7 is a random number in the range of $[0, 1]$, and p_m is the mutation probability. Through the above stages, the whole process of the MGPSO algorithm is completed and its flowchart is shown in Figure 3.

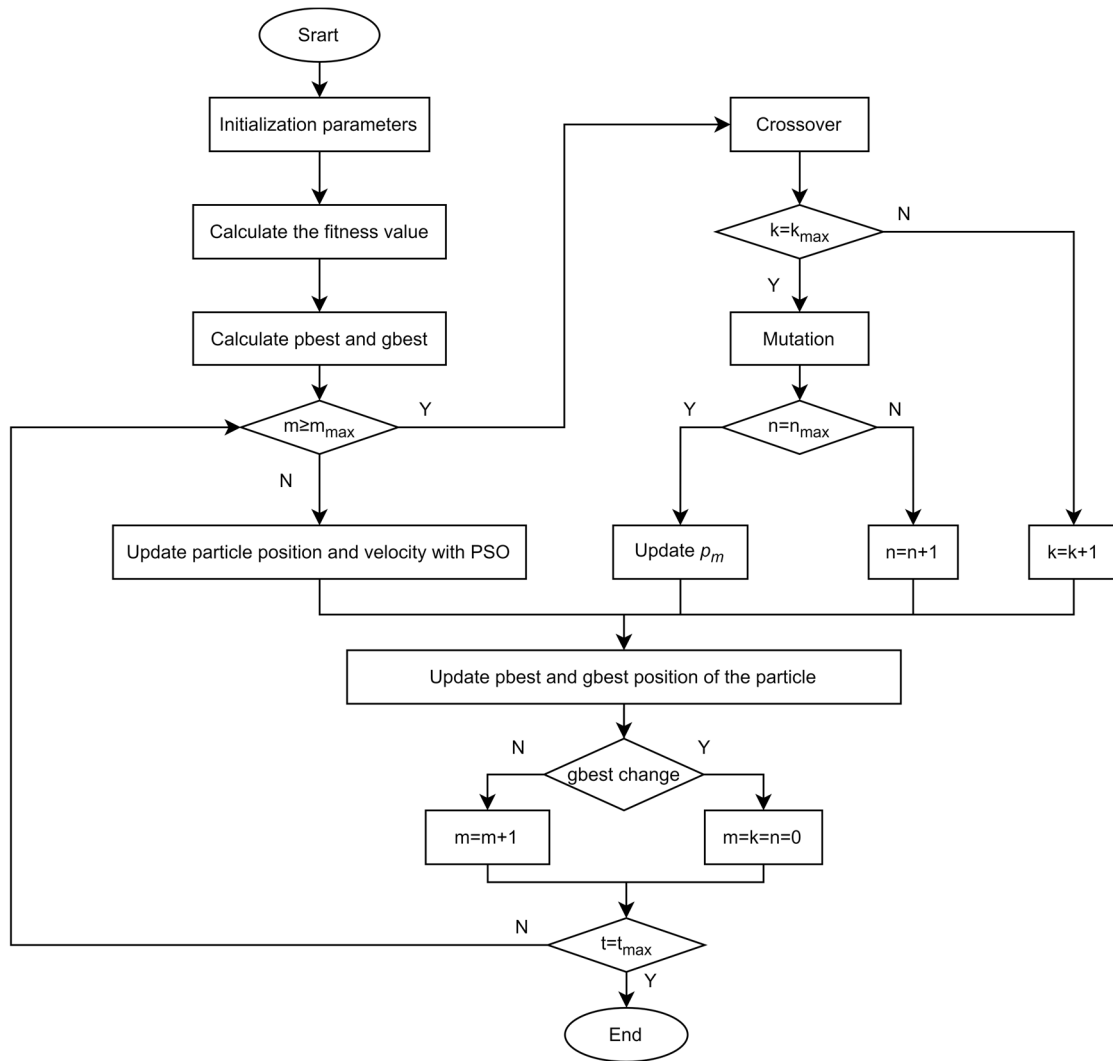


Figure 3. Flowchart of MGPSO.

4. Numerical Simulation

In the numerical simulation, the efficiency of the proposed MGPSO algorithm and the chromatography signal denoising algorithm for MGPSO-ITF are verified. The specific steps are shown in Figure 4, which is key to guiding the subsequent work.

4.1. Preparation Phase

First of all, we need to explain some necessary preliminary preparations. In actual engineering, chromatographic peaks commonly have a tailing phenomenon. Related studies have shown that the exponentially modified Gaussian function model can reasonably simulate chromatographic signals. The mathematical model is as follows:

$$h(t) = \frac{S}{\tau\sqrt{\pi}} \exp\left(\frac{\sigma^2}{2\tau^2} - \frac{t-t_g}{\tau}\right) \int_{-\infty}^z \exp(-x^2) dx \tag{22}$$

$$z = \left(\frac{t-t_g}{\sigma} - \frac{\sigma}{\tau}\right) / \sqrt{2} \tag{23}$$

where $h(t)$ is the peak height as a function of outflow time, S is the peak area, σ and t_g are the standard deviation of Gaussian peaks with center position time, and τ is the exponential correction time constant that determines the degree of peak trailing. The simulated signal constructed according to this method is shown in Figure 5.

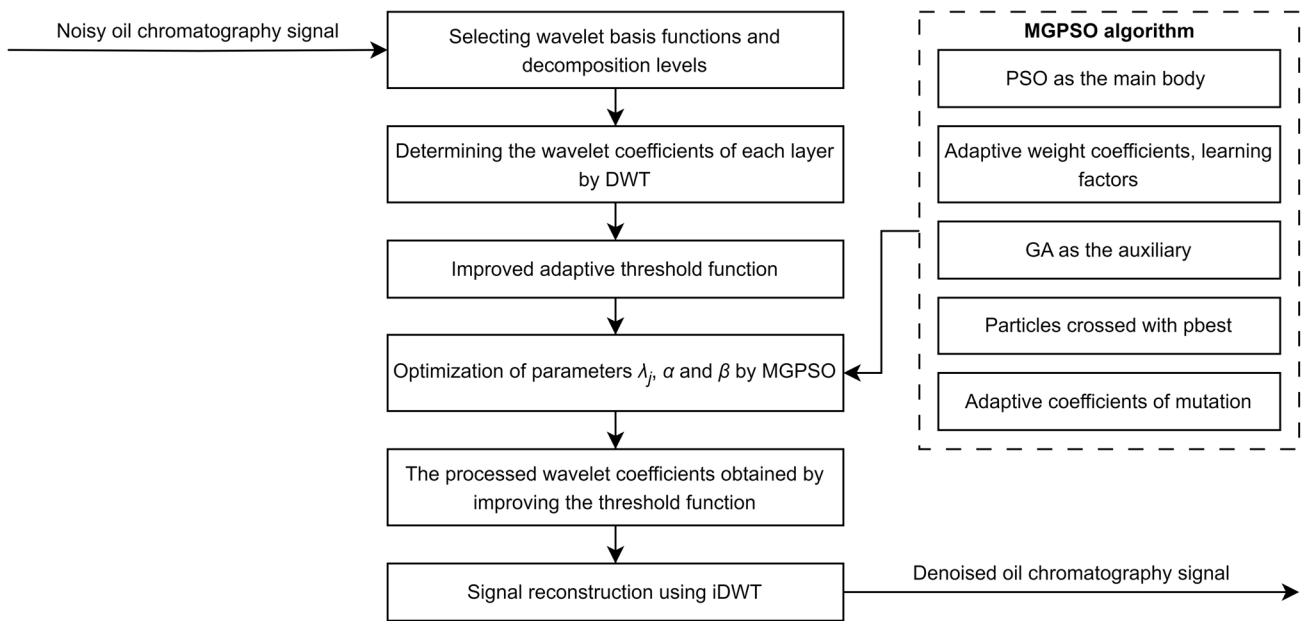


Figure 4. Flowchart of signal denoising using MGPSO-ITF.

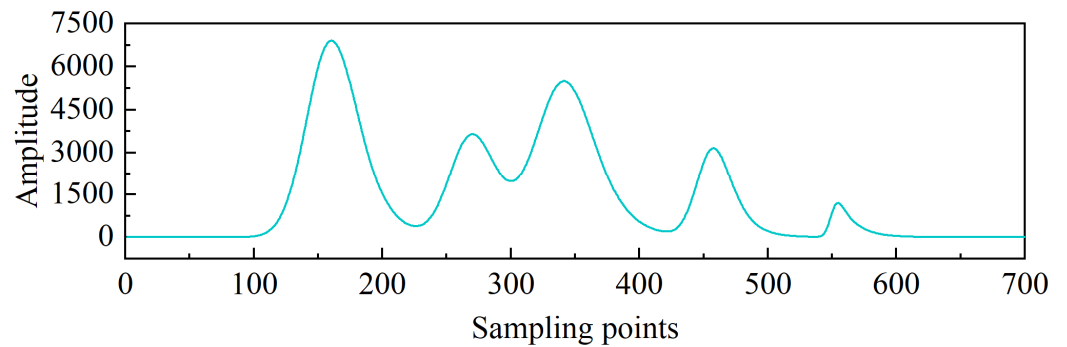


Figure 5. The simulated signal.

Subsequently, in view of visually comparing the denoising effects of different methods on analog signals, the following three evaluation metrics are introduced:

$$SNR = 10 \lg \frac{\sum_{i=1}^N f^2(i)}{\sum_{i=1}^N [f(i) - f'(i)]^2}, \tag{24}$$

$$RMSE = \sqrt{\frac{1}{N} \sum_{i=1}^N (f(i) - f'(i))^2}, \tag{25}$$

$$NSR = \frac{\sum_{i=1}^N (f(i) - \bar{f}(i)) (f'(i) - \bar{f}'(i))}{\sqrt{\sum_{i=1}^N [f(i) - \bar{f}(i)]^2 \times \sum_{i=1}^N [f'(i) - \bar{f}'(i)]^2}}, \tag{26}$$

where $f(i)$ is the original signal, $f'(i)$ is the reconstructed signal after denoising, $\bar{f}(i)$ and $\bar{f}'(i)$ represents the average values, respectively, and N is the signal length. The higher the SNR and the smaller the $RMSE$, the better the denoising effect. In particular, the closer the NSR is to 1, the closer the reconstructed signal is to the original signal.

4.2. Simulated Results of the MGPSO

The fitness value is a scalar used to measure the degree of superiority or inferiority of the particles in the iterative optimization process. In this paper, *MSE* is used as the fitness function, as shown in Equation (27):

$$MSE = \frac{1}{N} \sum_{i=1}^N (f(i) - f'(i))^2, \tag{27}$$

According to the corresponding parameter settings in DWT, the search space and position of the MGPSO are initialized, and the noisy signal is decomposed using a db7 wavelet basis with four decomposition layers. The process of determining these parameters is shown in Figures 6–8. The db7 has the highest SNR and the lowest RMSE among the three wavelet bases as in Figures 6 and 7, while the best denoising performance is achieved when the number of decomposition layers is four as in Figure 8. Therefore, the db7 wavelet base and four decomposition layers are used as parameters for subsequent signal processing.

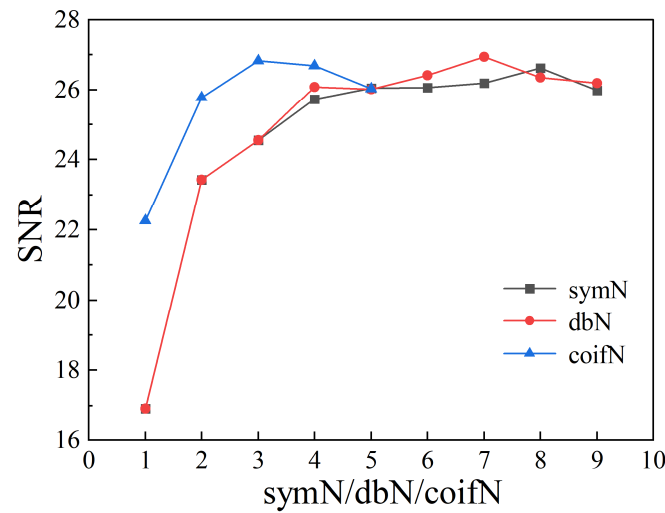


Figure 6. SNR under different wavelet base treatments.

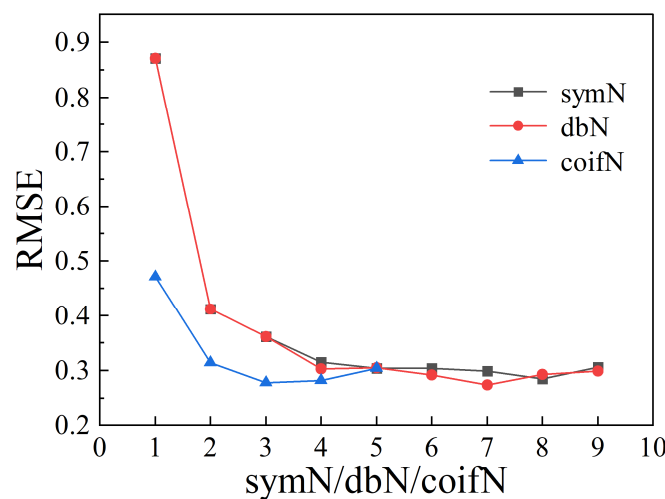


Figure 7. RMSE under different wavelet base treatments.

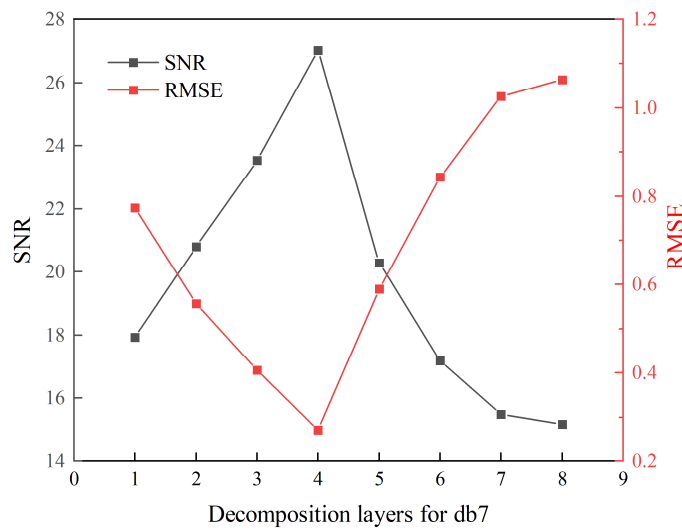


Figure 8. SNR and RMSE at different decomposition levels of db7.

The undefined parameters α, β, λ , although not reflected in Equation (27), are known from Equation (7) and the discrete inverse wavelet transform. The vector composed of α, β, λ is taken as the particle position of MGPSO, i.e., $(\alpha, \beta, \lambda_1, \lambda_2, \lambda_3, \lambda_4)$ with dimension 6. It is generally believed that the population size is twice or more than twice the dimension of the search space, so 12 is taken. The settings of the shape adjustment parameter α and the approximation speed parameter β are initialized from 1 to 50, while the threshold $\lambda_1, \lambda_2, \lambda_3, \lambda_4$ is initialized from 1 to 100. In order to verify the effectiveness of MGPSO, four PSO-related algorithms are selected for comparative testing. The relevant parameter settings of the algorithms are shown in Table 1.

Table 1. Parameter settings.

Algorithm	Parameter Setting
PSO	$w = 0.8, c_1 = c_2 = 2$
CPSO	$w = 1, c_1 = c_2 = 1.49, u = 0.9$, with Logistic as the mapping equation
GPSO [33]	$w_{\max} = 0.9, w_{\min} = 0.4, c_1 = c_2 = 1.49$
MPSO [28]	$w_{\max} = 0.9, w_{\min} = 0.4, c_{1\max} = c_{2\max} = 2.5, c_{1\min} = c_{2\min} = 0.5, p_m = 0.02$
MGPSO	$w_{\max} = 0.9, w_{\min} = 0.4, c_{1\max} = c_{2\max} = 2, c_{1\min} = c_{2\min} = 0.8$

The hardware of the simulation test platform is an Intel i5–13500 hx CPU, 16 GB RAM computer, and the software is MATLABR2022a based on the Window11 operating system. The simulation results prove that MGPSO has excellent convergence ability and good robustness in parameter optimization of wavelet threshold function. Its optimization iteration effect is shown in Figure 9, and it can be observed intuitively that MGPSO has the fastest convergence speed and the best iterative result. At around $t = 70$, while the other algorithms remain suboptimal, MGPSO can escape local optima and achieve a smaller MSE, facilitated by the integration of GA. This improvement is due to the synergistic combination of the two optimization methods, which allows for more effective exploration and exploitation of the search space.

In order to eliminate the influence of chance on the results, the optimal value, average value, median, and standard deviation of each algorithm in 50 experiments were used as the evaluation index of algorithm performance, and the recorded data are shown in Table 2. From the table, it can be found that the optimal value of MGPSO is the smallest. MGPSO has the strongest potential to search for optimal parameters according to the physical meaning of MSE, the highest convergence accuracy based on the smallest mean value, and excellent robustness because of the small standard deviation value. In summary, the superiority of MGPSO is verified.

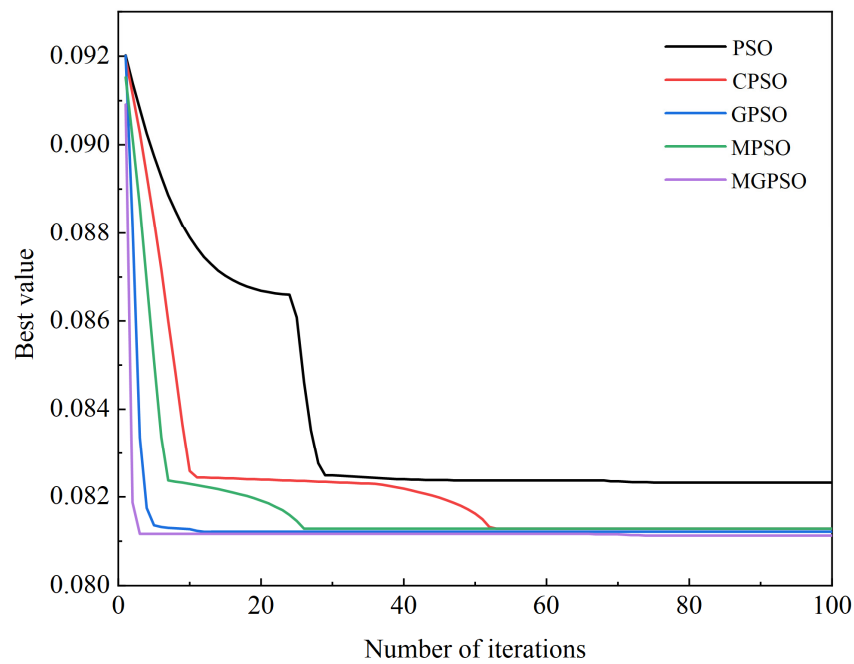


Figure 9. Threshold parameter optimization seeking iteration curve.

Table 2. Wavelet threshold parameter search performance.

Algorithm	Optimal Value	Mean	Median	Standard Deviation
PSO	0.0823	0.0838	0.0824	0.0026
CPSO	0.0813	0.0823	0.0816	0.0020
MPSO	0.0812	0.0814	0.0812	0.0013
GAPSO	0.0813	0.0818	0.0813	0.0017
MGPSO	0.0811	0.0812	0.0811	0.0009

4.3. Simulated Results of the MGPSO-ITF

In order to verify the denoising effect of MGPSO-ITF, the simulated signal experiments with 15db added Gaussian white noise and their results are compared with the processing results of traditional hard thresholding and soft thresholding, as shown in Table 3. The SNR and NSR of the improved thresholding function proposed in this paper are significantly higher than the traditional hard and soft thresholding functions, proving the effectiveness of the method.

Table 3. Threshold function denoising index.

Index	Hard Threshold	Soft Threshold	Improved Threshold	Noise SNR (db)
SNR	21.8398	24.6049	26.6134	15
RMSE	0.4937	0.3591	0.2849	
NSR	0.9948	0.9972	0.9984	

Figure 10 shows the filtering effect of the original signal plus 15 db noise. The figure shows that the denoising effect of the hard thresholding method is not ideal, and there are obvious oscillations; the soft thresholding function can denoise the signal smoothly, but it leads to the loss of too many details of the signal. The processing result of MGPSO-ITF is smooth and the reconstruction accuracy is high. Specifically, for the originally relatively smooth signal, MGPSO-ITF does not over-correct it to cause distortion, which is extremely important for reconstructing the signal quality, which is also a specific embodiment of the soft thresholding shortcomings. Therefore, MGPSO-ITF has the best denoising effect.

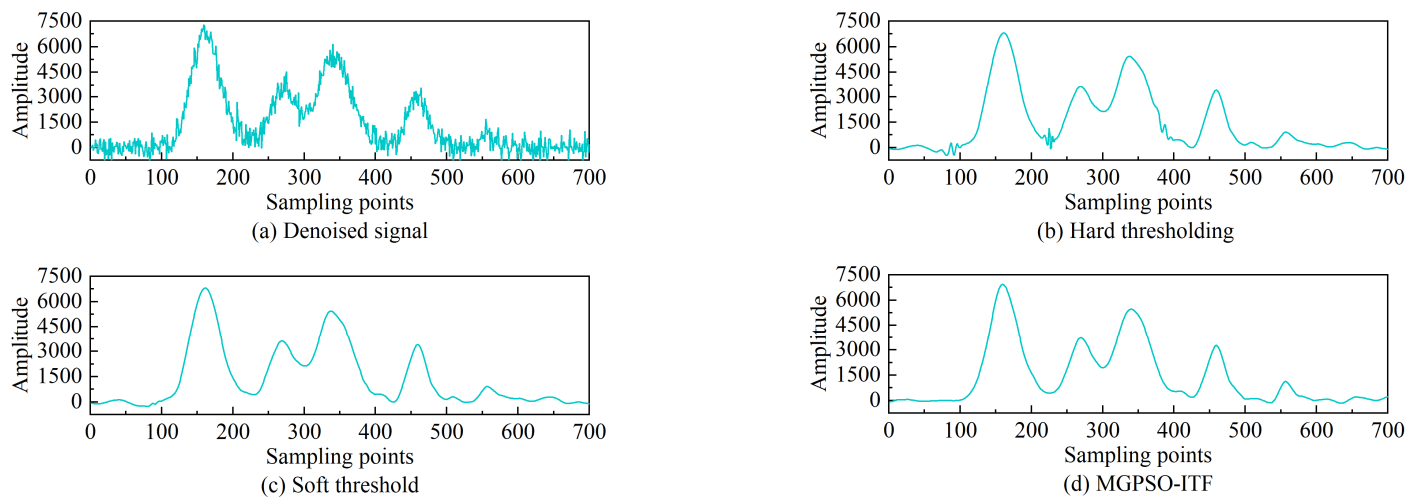


Figure 10. Simulated signal denoising effect.

In order to analyze the effect more comprehensively, we added different degrees of Gaussian white noise to the simulated signals and introduced six other improved threshold function methods to compare with the denoising effect of MGPSO. The relevant parameter settings of these algorithms are shown in Table 4.

Table 4. Parameter settings in Figure 11.

Algorithm	Parameter Setting in the Threshold Function
MGPSO-ITF	$\alpha = 4.1, \beta = 5.11$
Ref. [18]	$a \leq 1/\lambda^2$
Ref. [19]	None
Ref. [28]	$\alpha = 30$
Ref. [29]	$\alpha = 1.2, \beta = 0.25$
Ref. [30]	$\eta = 10$
Ref. [34]	$k = 11.5$

As seen in Figure 11, Ref. [28] has achieved satisfactory denoising performance at low SNR but has the problem of insufficient signal information preservation when SNR becomes high. Ref. [30] can occasionally obtain better denoising results, but its stability is unsatisfactory. These phenomena are caused by the inappropriate selection of threshold function parameters due to the optimization algorithm falling into a local optimum. Ref. [19] has better stability but inadequate adaptivity due to a lack of adjustment parameters. The performance of Refs. [18,29,34] tends to stabilize as the input SNR increases, but the final denoising effect is not as significant as MGPSO-ITF. In contrast, the proposed MGPSO-ITF algorithm outperforms the existing approaches in terms of output SNR, RMSE, and NSR. At low input SNR levels, most algorithms encounter difficulties in extracting signal components due to the overwhelming presence of noise. However, MGPSO-ITF exhibits improved differentiability and continuity, facilitating clearer extraction of the original signal within the noisy environment. This characteristic underscores the algorithm’s adaptability to challenging scenarios. As the input SNR level increases, the distinction between noise and signal energy becomes more pronounced. In such cases, MGPSO-ITF effectively segregates noise from the signal, resulting in superior denoising performance compared to other algorithms. These comparative findings accentuate the strengths and advantages of MGPSO-ITF over existing methods, highlighting its efficacy in noise handling and its preservation of signal characteristics across a broad range of SNR values.

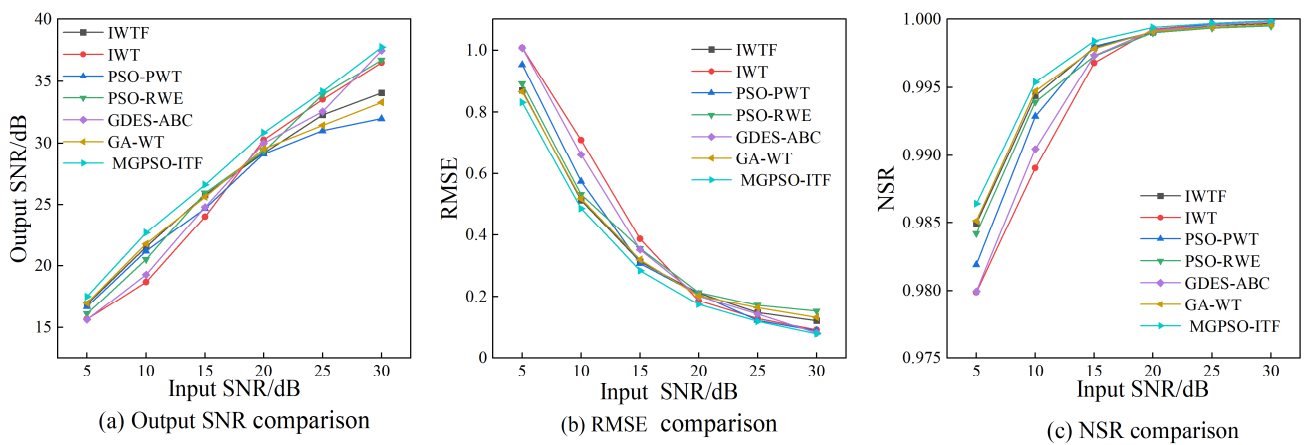


Figure 11. Denoising performance of different algorithms for different SNR inputs. (The methods and references in the figure are as follows: IWTF [18], IWT [19], PSO-PWT [28], PSO-RWE [29], GDES-ABC [30] and GA-WT [34].)

5. The Experiment on Measured Signals

5.1. Signal Measurement Equipment

In this section, the denoising performance of the proposed MGPSO-ITF algorithm is evaluated using measured chromatographic signals in actual engineering. The measured chromatographic signals in this paper were collected using the experimental platform shown in Figure 12. The intelligent electronic device (IED) is a new type of field data acquisition device that can remotely monitor the operating status of substations in real time and record, analyze, fit, and process field data. It can also interact with other data and upload the analyses results to the status-monitoring master station.

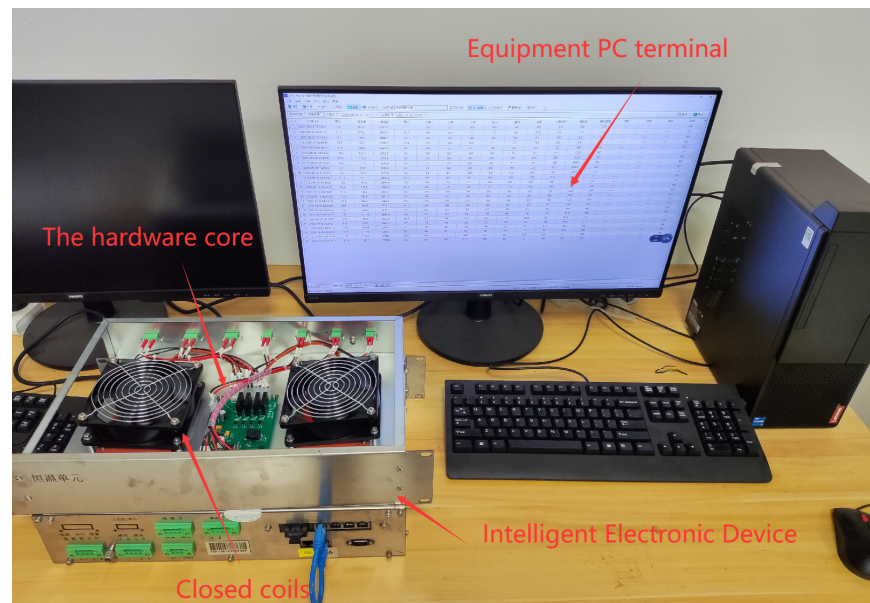


Figure 12. The experimental equipment.

5.2. Experimental Results

In actual engineering, commonly used chromatographic data processing methods also include the Fast Fourier Transform (FFT) and the Savitzky-Golay (S-G) methods, which will be compared with threshold denoising. As shown in Figure 13, the results of hard thresholding are very suboptimal, with too many glitches. The soft thresholding results in noticeable distortion and excessive glitches. After filtering using the FFT method, the signal distortion is the most significant. The signal after the S g is not smooth, which is

caused by the inappropriate choice of window length. The improved threshold algorithm has demonstrated superior denoising performance, yielding a signal curve that is notably smoother with fewer glitches and only minimal distortion. Moreover, the algorithm has also shown improved smoothing effects in the gentle region, which can be attributed to the optimization of parameters. These results highlight the efficacy of the improved threshold algorithm in enhancing the quality of the processed signal.

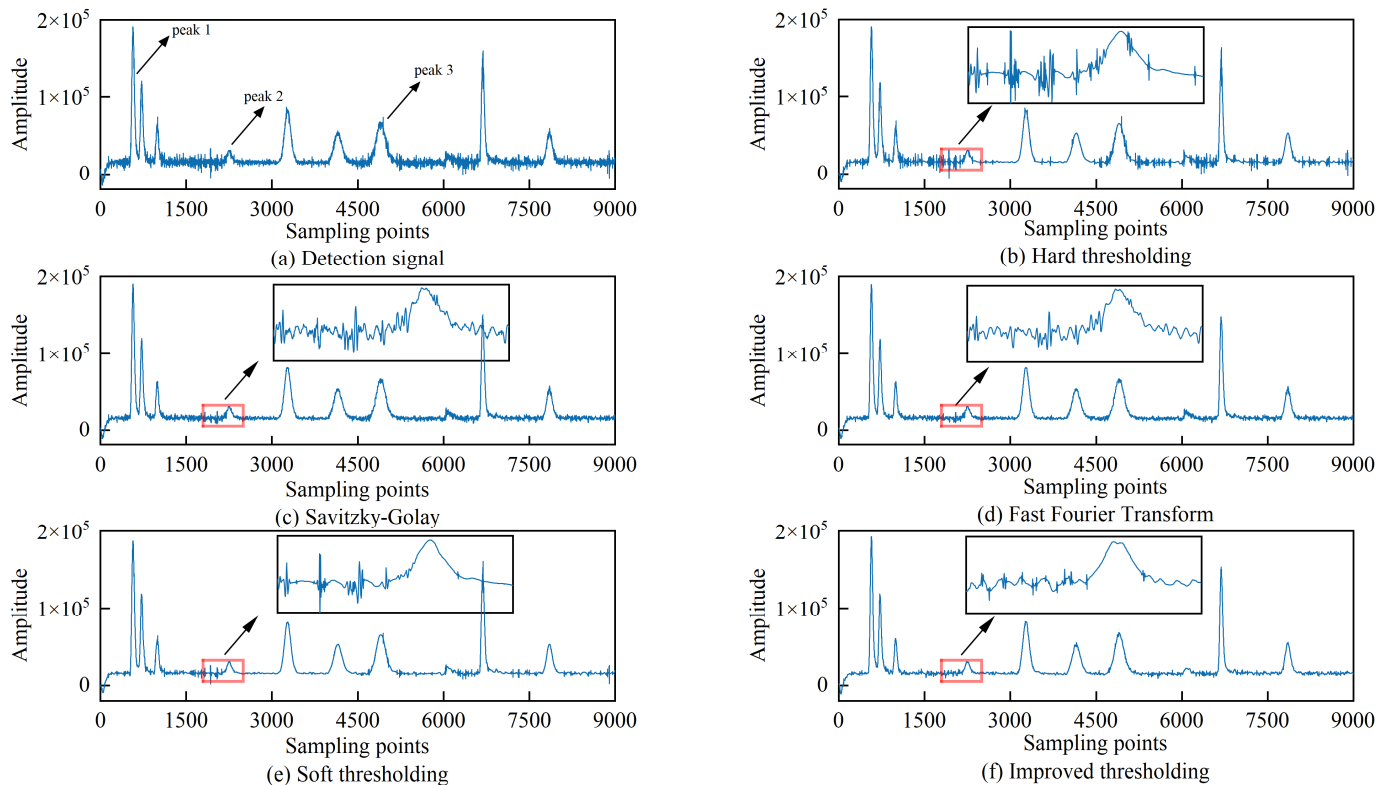


Figure 13. Denoising effect of chromatographic signal.

Quantitative evaluation of the denoising performance using numerical metrics such as SNR and RMSE is limited by the unavailability of the ideal noise-free signal. As such, alternative methods must be employed to reliably assess the effectiveness of the denoising algorithm. For oil chromatography signals in engineering, the peak is valuable, filtering results in enlarged peak areas and decreased chromatographic peak height. Figure 13 does not clearly show the deviation and loss of peak characteristics; so, the peak area distortion can be used to evaluate the denoising effect. The peak area reflects the composition content of the substance that is to be measured, which is of great significance in chromatographic analysis. The lower the peak area distortion, the better the denoising effect. Peak area and distortion are calculated as follows:

$$S = W \times H, \quad (28)$$

$$\Delta S = \left| \frac{(S_o - S_d)}{S_o} \right| \times 100, \quad (29)$$

where W is the half-peak width and H is the peak height. Since S_g and FFT cause severe peak distortion, quantitative calculations are not performed here. After processing the three typical peaks in Figure 13, the evaluation indexes are shown in Table 5.

Table 5. Chromatographic peak evaluation index.

Denoising Method	Peak Area Distortion Rate (%)		
	Peak 1	Peak 2	Peak 3
Hard threshold	4.893	8.548	1.624
Soft threshold	5.336	6.669	1.901
Improved threshold	4.518	5.614	1.017

Generally speaking, the distortion rate is kept within 5%, which is an acceptable range. The data in Table 5 illustrates that the peak area of soft thresholding has the highest distortion rate, while MGPSO-ITF has the lowest. However, at peak 2, after hard thresholding, the burr leads to incorrect identification of the peak starting point, resulting in the most significant error. In particular, all three thresholding treatments exceed 5%, which indicates that there is also much room for improvement in MGPSO-ITF.

6. Conclusions

In the DGA process, the denoised oil chromatographic signals have a significant impact on the qualitative and quantitative analysis of signals. The selection of an appropriate wavelet basis function and the number of decomposition layers are crucial, and analytical calculations are employed to determine these parameters accurately. Furthermore, an enhanced denoising approach using an adaptive wavelet threshold function (MGPSO-ITF) is proposed in this paper. Through mathematical proof and simulation experiments, several important conclusions can be drawn. Firstly, the proposed method overcomes the limitations of hard and soft thresholding by employing a constructional approach for the parametric wavelet thresholding function. This enables more effective denoising of the signals. Moreover, the MGPSO algorithm exhibits excellent performance in terms of convergence, stability, and global search capability. It addresses the drawbacks of fixed thresholding and enhances the interpretability of adjustment parameters found in traditional algorithms. The presented simulation results and actual engineering applications demonstrate the superiority of the MGPSO-ITF method in denoising oil-chromatography signals when compared to other algorithms. In the future, the algorithm will be further refined to enhance its denoising effectiveness and improve its applicability in actual engineering applications.

Author Contributions: Conceptualization, Z.F.; methodology, J.Z.; validation, J.Z.; formal analysis, J.Z.; data curation, K.L. and A.S.; writing—original draft preparation, J.Z.; writing—review and editing, Z.F., K.L., A.S.; visualization, J.Z.; supervision, Z.F.; funding acquisition, Z.F. All authors have read and agreed to the published version of the manuscript.

Funding: This research received no external funding.

Data Availability Statement: The data can be shared up on request.

Acknowledgments: We thank L.Z. and Y.W. for writing—review and editing.

Conflicts of Interest: The authors declare no conflict of interest.

Abbreviations

a	The scaling factor
b	The translation factor
$d_{j,k}$	The high-frequency coefficients
$a_{j,k}$	The low-frequency coefficients
f_i	The chromatographic signal
x_i	The pure signal
s_i	The background noise

N	The total number of samples
$w_{j,k}$	The original wavelet coefficient
$\hat{w}_{j,k}$	The processed wavelet coefficient
λ	The threshold
t	The current number of iterations
j	The current solution space
r	A random number
w	The inertia weight coefficient
c	The learning factors
x_{ij}^t	The particle position
v_{ij}^t	The particle velocity
p_m	The mutation probability
$h(t)$	The peak height
S	The peak area
t_g	The standard deviation
τ	The exponential correction time

References

- Jin, Y.S.; Wu, H.; Zheng, J.F.; Zhang, J.; Liu, Z. Power Transformer Fault Diagnosis Based on Improved BP Neural Network. *Electronics* **2023**, *12*, 3526. [CrossRef]
- Liu, W.K.; Zhang, Z.G.; Zhang, J.R.; Huang, H.X.; Zhang, G.C.; Peng, M.D. A Novel Fault Diagnosis Method of Rolling Bearings Combining Convolutional Neural Network and Transformer. *Electronics* **2023**, *12*, 1838. [CrossRef]
- Yang, P.J.; Wang, T.Y.; Yang, H.; Meng, C.P.; Zhang, H.; Cheng, L. The Performance of Electronic Current Transformer Fault Diagnosis Model: Using an Improved Whale Optimization Algorithm and RBF Neural Network. *Electronics* **2023**, *12*, 1066. [CrossRef]
- Cui, H.Z.; Yang, L.Q.; Zhu, Y.W.; Li, S.T.; Abu-Siada, A.; Islam, S. Dissolved Gas Analysis for Power Transformers within Distributed Renewable Generation-Based Systems. *IEEE Trans. Dielectr. Electr. Insul.* **2021**, *28*, 1349–1356. [CrossRef]
- Su, R.; Wang, Z. Research of Wavelet De-noising Control for gamma Spectrum. *At. Energy Sci. Technol.* **2014**, *48*, 1309–1313.
- Vajpayee, V.; Mukhopadhyay, S.; Tiwari, A.P. Multiscale subspace identification of nuclear reactor using wavelet basis function. *Ann. Nucl. Energy* **2018**, *111*, 280–292. [CrossRef]
- da Silva, P.C.L.; da Silva, J.P.; Garcia, A.R.G. Daubechies wavelets as basis functions for the vectorial beam propagation method. *J. Electromagn. Waves Appl.* **2019**, *33*, 1027–1041. [CrossRef]
- Chanu, P.R.; Singh, K.M. A two-stage switching vector median filter based on quaternion for removing impulse noise in color images. *Multimed. Tools Appl.* **2019**, *78*, 15375–15401. [CrossRef]
- Vijaykumar, V.R.; Mari, G.S.; Ebenezer, D. Fast switching based median-mean filter for high density salt and pepper noise removal. *Int. J. Electron. Commun.* **2014**, *68*, 1145–1155. [CrossRef]
- Li, C.; Wu, Y.; Lin, H.; Li, J.; Zhang, F.; Yang, Y. ECG Denoising Method Based on an Improved VMD Algorithm. *IEEE Sens. J.* **2022**, *22*, 22725–22733. [CrossRef]
- Guillen, D.; Esponda, H.; Vazquez, E.; Idarraga-Ospina, G. Algorithm for transformer differential protection based on wavelet correlation modes. *IET Gener. Transm. Distrib.* **2016**, *10*, 2871–2879. [CrossRef]
- Gao, H.Y. Wavelet shrinkage denoising using the non-negative garrote. *J. Comput. Graph. Stat.* **1998**, *7*, 469–488.
- Chaari, L.; Ciuciu, P.; Meriaux, S.; Pesquet, J.C. Spatio-temporal wavelet regularization for parallel MRI reconstruction: Application to functional MRI. *Magn. Reson. Mater. Phys. Biol. Med.* **2014**, *27*, 509–529. [CrossRef] [PubMed]
- Qin, Y.; Mao, Y.F.; Tang, B.P. Multicomponent decomposition by wavelet modulus maxima and synchronous detection. *Mech. Syst. Sig. Process.* **2017**, *91*, 57–80. [CrossRef]
- Gu, J.; Lin, P.; Ling, B.W.-K.; Yang, C.; Feng, P. Grouping and selecting singular spectral analysis components for denoising based on empirical mode decomposition via integer quadratic programming. *IET Signal Proc.* **2018**, *12*, 599–604. [CrossRef]
- Kuang, W.; Wang, S.; Lai, Y.; Ling, W.-K. Efficient and Adaptive Signal Denoising Based on Multistage Singular Spectrum Analysis. *IEEE Trans. Instrum. Meas.* **2021**, *70*, 1–20. [CrossRef]
- Donoho, D.L. De-noising by Soft-Thresholding. *IEEE Trans. Inf. Theory* **1995**, *41*, 613–627. [CrossRef]
- Tong, Y.N.; Li, J.G.; Xu, Y.H.; Cao, L.C. Signal Denoising Method Based on Improved Wavelet Threshold Function for Microchip Electrophoresis (CD)-D-4 Equipment. *Complexity* **2020**, *2020*, 6481317. [CrossRef]
- Xie, B.; Xiong, Z.Q.; Wang, Z.J.; Zhang, L.J.; Zhang, D.Z.; Li, F.S. Gamma spectrum denoising method based on improved wavelet threshold. *Nucl. Eng. Technol.* **2020**, *52*, 1771–1776. [CrossRef]
- Sun, K.; Lu, Y.; Yang, X.; Huang, L.; Chen, X. Application of Modified Wavelet Threshold Function in High Power Supply Signal. *J. Power Supply* **2022**, 1–12. Available online: <https://kns.cnki.net/kcms/detail/12.1420.TM.20221206.1420.001.html> (accessed on 10 October 2023).

21. Zhou, F.B.; Li, C.G.; Zhu, H.Q. Research on Threshold Improved Denoising Algorithm Based on Lifting Wavelet Transform in UV-Vis Spectrum. *Spectrosc. Spectr. Anal.* **2018**, *38*, 506–510.
22. Li, X.X.; Liao, K.X.; He, G.X.; Zhao, J.H. Research on Improved Wavelet Threshold Denoising Method for Non-Contact Force and Magnetic Signals. *Electronics* **2023**, *12*, 1244. [[CrossRef](#)]
23. Zhang, X.P.; Desai, M.D. Adaptive denoising based on sure risk. *IEEE Signal Process Lett.* **1998**, *5*, 265–267. [[CrossRef](#)]
24. Yang, Y.; Wei, Y.S.; Yang, M. Signal Denoising Based on the Adaptive Shrinkage Function and Neighborhood characteristics. *Circuits, Syst. Signal Process.* **2014**, *33*, 3921–3930. [[CrossRef](#)]
25. Solis, M.; Ma, Q.; Galvin, P. Damage detection in beams from modal and wavelet analysis using a stationary roving mass and noise estimation. *J. Strain Anal. Eng. Des.* **2018**, *54*, e12266. [[CrossRef](#)]
26. Yang, Y.; Wei, Y.S. An adaptive shrinkage function for image denoising based on neighborhood characteristics. *Image Anal. Stereol.* **2022**, *41*, 121–131. [[CrossRef](#)]
27. Bhutada, G.G.; Anand, R.S.; Saxena, S.C. PSO-based learning of sub-band adaptive thresholding function for image denoising. *Signal Image Video Process* **2012**, *6*, 1–7. [[CrossRef](#)]
28. Zhang, X.; Li, J.L.; Xing, J.C.; Wang, P.; Yang, Q.L.; He, C. A Particle Swarm Optimization Technique-Based Parametric Wavelet Thresholding Function for Signal Denoising. *Circuits Syst. Signal Process.* **2017**, *36*, 247–269. [[CrossRef](#)]
29. Yang, X.; Qiu, M.; Chen, L.; Chen, Y. Adaptive wavelet threshold function based on pso-rwe for vibration signal denoising of rolling bearing. *J. Aerosp. Power* **2020**, *35*, 2339–2347. [[CrossRef](#)]
30. Wang, J.; Li, J.; Yan, S.; Shi, W.; Yang, X.; Guo, Y.; Gulliver, T.A. A Novel Underwater Acoustic Signal Denoising Algorithm for Gaussian/Non-Gaussian Impulsive Noise. *IEEE Trans. Veh. Technol.* **2021**, *70*, 429–445. [[CrossRef](#)]
31. Duan, B.; Guo, C.; Liu, H. A hybrid genetic-particle swarm optimization algorithm for multi-constraint optimization problems. *Soft Comput.* **2022**, *26*, 11695–11711. [[CrossRef](#)]
32. Xu, F.; Zou, D.; Li, C.; Luo, H.; Zhang, M. Improved Particle Swarm Optimization Algorithm with Circle Mapping and Sine Cosine Factor. *Comput. Eng. Appl.* **2023**, 80–90. Available online: <https://kns.cnki.net/kcms/detail/11.2127.TP.20230224.1812.016.html> (accessed on 10 October 2023).
33. Zhang, Z.M. Abnormal Detection of Pumping Unit Bearing Based on Extension Theory. *IEEJ Trans. Electr. Electron. Eng.* **2021**, *16*, 1647–1652. [[CrossRef](#)]
34. Yang, G.; Dai, J.; Liu, X.; Wu, X.; Chen, M.; Qin, H. Denoising of gamma-ray spectrum by optimized wavelet thresholding based on modified genetic algorithm in carbon/oxygen logging. *J. Radioanal. Nucl. Chem.* **2019**, *320*, 351–359. [[CrossRef](#)]

Disclaimer/Publisher’s Note: The statements, opinions and data contained in all publications are solely those of the individual author(s) and contributor(s) and not of MDPI and/or the editor(s). MDPI and/or the editor(s) disclaim responsibility for any injury to people or property resulting from any ideas, methods, instructions or products referred to in the content.